

Advancing Depth Anything Model for Unsupervised Monocular Depth Estimation in Endoscopy

Bojian Li¹, Bo Liu¹, Xinning Yao¹, Jinghua Yue¹, and Fugen Zhou¹

Abstract—Depth estimation is a cornerstone of 3D reconstruction and plays a vital role in minimally invasive endoscopic surgeries. However, most current depth estimation networks rely on traditional convolutional neural networks, which are limited in their ability to capture global information. Foundation models offer a promising approach to enhance depth estimation, but those models currently available are primarily trained on natural images, leading to suboptimal performance when applied to endoscopic images. In this work, we introduce a novel fine-tuning strategy for the Depth Anything Model and integrate it with an intrinsic-based unsupervised monocular depth estimation framework. Our approach includes a low-rank adaptation technique based on random vectors, which improves the model’s adaptability to different scales. Additionally, we propose a residual block built on depthwise separable convolution to compensate for the transformer’s limited ability to capture local features. Our experimental results on the SCARED dataset and Hamlyn dataset show that our method achieves state-of-the-art performance while minimizing the number of trainable parameters. Applying this method in minimally invasive endoscopic surgery can enhance surgeons’ spatial awareness, thereby improving the precision and safety of the procedures.

I. INTRODUCTION

Depth estimation is a crucial component of augmented reality navigation systems in minimally invasive endoscopic surgery, where accurate 3D depth information is essential for enhancing surgical precision and safety [1], [2]. Given the difficulties in obtaining ground truth from endoscopic images and the fact that monocular endoscopes are more flexible and practical compared to stereo endoscopes, unsupervised monocular depth estimation (UMDE) algorithms have attracted broader research interest [3], [4]. These algorithms typically transform the depth estimation task into an image synthesis problem between adjacent viewpoints, using image synthesis error to guide network training [5]. However, conventional depth estimation algorithms face significant challenges when applied to endoscopic images due to factors such as lighting variations and sparse textures [6].

To address the challenges of UMDE in endoscopy, particularly those related to lighting variations, several approaches have been proposed. For instance, AF-SfMLearner [7] designs an appearance flow extraction network for nonlinear adjustment of image lighting. IID-SfMLearner [6] combines



Fig. 1. Left: endoscopic image from minimally invasive surgery scenes. Middle: depth estimation result from Depth Anything Model [12]. Right: more accurate depth estimation result from our model.

image intrinsic decomposition with depth estimation, incorporating reflectance invariance to supervise network training. These strategies have significantly improved the performance of monocular endoscopic depth estimation. However, the depth estimation networks in these methods rely on simple convolutional neural networks, which primarily capture local information and are limited in their ability to perceive global information.

The emergence of foundation models has sparked a new revolution in the field of computer vision [8], [9]. These models, often based on Vision Transformers (ViT), excel at effectively extracting global image features. For dense prediction tasks like semantic segmentation and depth estimation, having a global receptive field for each pixel relative to the scene allows the network to estimate local information with greater accuracy [10]. Moreover, these models are typically trained on extremely large-scale datasets, endowing them with robust zero- and few-shot capabilities across a wide range of downstream scenarios [11].

Recently, a foundation model (Depth Anything Model) for depth estimation in natural images has been proposed [12]. However, as shown in Fig. 1, this model exhibits significant performance degradation when directly applied to endoscopic images [13]. Furthermore, due to the scarcity of annotated endoscopic data, training a foundation model for endoscopic depth estimation from scratch is impractical. Therefore, fine-tuning the Depth Anything Model for specific endoscopic scenarios has become an effective approach to addressing this issue.

There are numerous strategies for fine-tuning foundation models, with Low-Rank Adaptation (LoRA) being one of the most commonly used methods [14]. However, LoRA does not always perform optimally and some variations show better performance in certain tasks. To address this, we explore a novel fine-tuning strategy aimed at enhancing performance without increasing the number of parameters in LoRA. Inspired by recent studies that highlight the surprising effectiveness of models using random weights and projec-

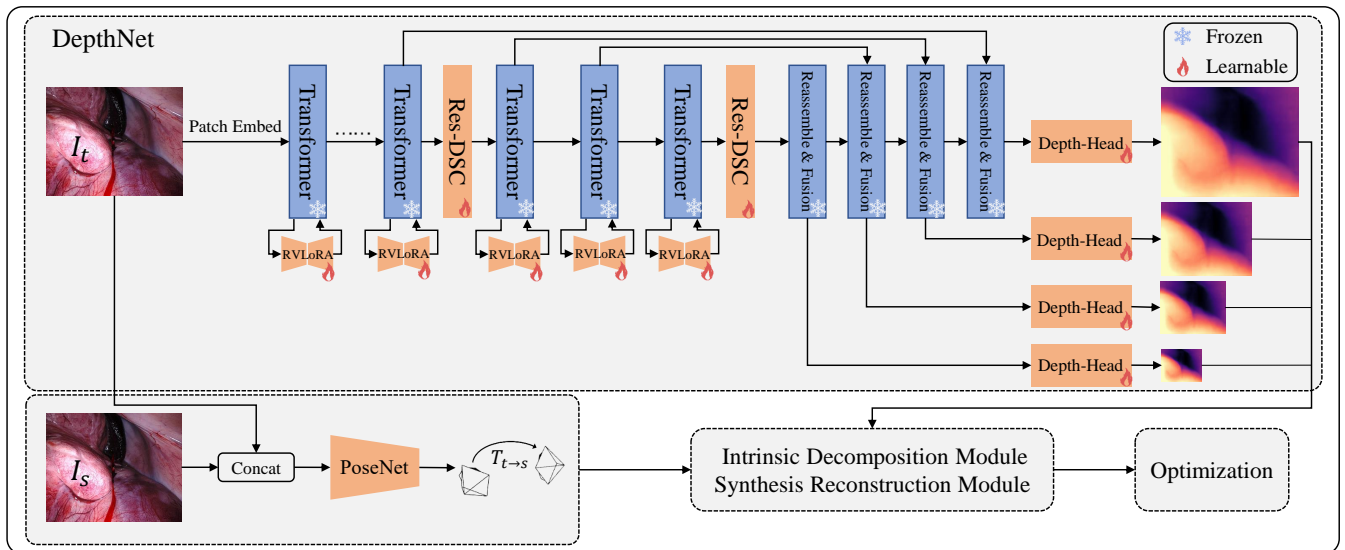


Fig. 2. Network architecture diagram. The encoder in the depth network contains 12 transformer modules, each with an RVLoRA module. Res-DSC modules are added after the 3rd, 6th, 9th, and 12th layers.

tions [15], [16], we propose a low-rank adaptation method based on random vectors (RVLoRA) that enhances model performance without adding additional trainable parameters. Additionally, transformer models tend to focus more on low-frequency information, resulting in insufficient ability to extract texture details and local features [17], [18]. To address this, we propose a residual block based on depthwise separable convolution (Res-DSC) to achieve higher performance by enhancing locality.

In summary, our main contributions are as follows:

- We designed a novel fine-tuning strategy, RVLoRA, for depth estimation foundation model. This strategy enhances the model’s adaptability to different scales by introducing random scaling vectors, without adding additional trainable parameters.
- We introduced the Res-DSC module, which integrates a CNN component into the Vision Transformer (ViT), thereby improving the model’s ability to capture local features.
- Experiments conducted on SCARED dataset and Hamlyn dataset demonstrate that our approach achieves state-of-the-art results with the minimal trainable parameters.

II. RELATED WORKS

A. Unsupervised Monocular Depth Estimation

UMDE has been effectively explored on natural images. Zhou et al. [4] were the first to propose using view synthesis for UMDE. Subsequently, Godard et al. [5] further enhanced the performance by utilizing per-pixel loss minimization and automatic masking. Zheng et al. [19] improved depth estimation in nighttime scenarios by jointly learning image enhancement and depth estimation.

Despite the advances these methods have made for natural images, most of them rely on the assumption of photometric

consistency, which renders them less effective in endoscopic scenarios with varying illumination. To address this, Ozyoruk et al. [20] and Shao et al. [7] first adjusted the lighting of images before performing depth estimation. Li et al. [6] improved the results by employing intrinsic decomposition to separate illumination variations and using reflectance consistency. Besides this line of research, Battle et al. [21] used photometric stereo technique to achieve depth estimation of the human colon, but this method only performed well on the cavitory endoscope dataset. Cui et al. [13] combined foundation model techniques for depth estimation, achieving relatively better results.

B. Low-Rank Adaptation

LoRA [14] marked a significant breakthrough in efficiently training large language models for specific tasks by decomposing matrices into two low-rank matrices, A and B, thereby drastically reducing training resource consumption. Based on this idea, several improvements have been proposed recently. For example, LoRA+ [22] further enhanced efficiency by introducing different learning rates for matrices A and B. Zhang et al. [23] introduced AdaLoRA, which selects different ranks for different adapters. This method effectively enhances LoRA’s learning capability and training stability. VeRA [15] reduced the parameter count even further by freezing matrices A and B and introducing additional vectors for training, though this led to a slight loss in accuracy. Different fine-tuning strategies exhibit varying performance across different tasks. Therefore, we need to explore a fine-tuning strategy that is suitable for depth estimation tasks.

III. METHOD

In this section, we first review the framework of image intrinsic-based unsupervised monocular depth estimation, which serves as the baseline for our method. We then describe how we fine-tune the foundational model to obtain

a better depth estimation. Fig. 2 illustrates our network framework.

A. Image Intrinsic-Based UMDE

In classic UMDE framework [4], taking one frame as the target image I_t and adjacent frames as source images I_s , a depth estimation network is used to estimate the depth information D_t of the target image, and a pose estimation network is used to estimate the camera’s pose transformation matrix $T_{t \rightarrow s}$ between adjacent frames. Using known camera intrinsic matrix K , the position correspondence between the I_t and I_s is determined:

$$p_s \sim K T_{t \rightarrow s} D_t(p_t) K^{-1} p_t \quad (1)$$

here, p_t and p_s represent the pixel coordinates of the same point in three-dimensional space under the target view and the source view, respectively. Based on these, a synthesized frame $I_{s \rightarrow t}$ can be reconstructed via image warping. And the photometric loss between the reconstructed image $I_{s \rightarrow t}$ and the real target image I_t is calculated to supervise network training which is commonly constructed as a weighted combination of L1 loss and SSIM loss.

This framework relies on the assumption of photometric consistency, which no longer holds in endoscopy. IID-SfMLearner [6] employs intrinsic image decomposition to tackle the challenge, making it the most advanced framework for monocular endoscopic depth estimation. IID-SfMLearner additionally introduces the intrinsic decomposition module and synthetic reconstruction module to perform image decomposition and refine the decomposition results. This allows the method to leverage the inherent reflectance consistency of images, providing better supervision during network training.

B. Advancing Depth Anything Model for UMDE

The depth estimation networks typically employed in IID-SfMLearner and other classic UMDE methods are standard convolutional neural networks, which lack sufficient global perception capabilities for accurately capturing depth information. Fine-tuning a foundation model is a straightforward approach to enhance long-range dependencies without significantly increasing the number of trainable parameters. Although the Depth Anything Model [12] has been proposed for depth estimation, it was trained on natural images, and applying it directly to endoscopic images leads to poor performance. To address this, we propose a novel fine-tuning strategy specifically tailored for endoscopic images. Our approach introduces two key components: low-rank adaptation based on random vectors and residual blocks utilizing depthwise separable convolution.

1) *Low-rank Adaptation Based on Random Vectors (RVLoRA)*: As models grow larger, full fine-tuning becomes increasingly impractical. Neural networks consist of many dense layers that perform matrix multiplications, and the weight matrices in these layers are typically full-rank. However, when adapting to specific tasks, pre-trained foundation models exhibit low "intrinsic dimensions" [24]. This means

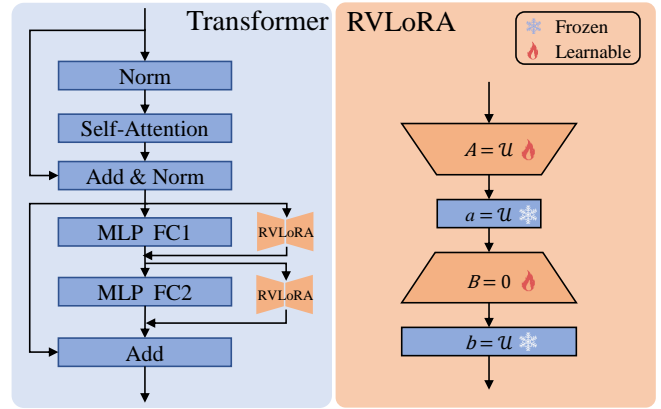


Fig. 3. The deployment and detailed structure of the RVLoRA. RVLoRA is connected to the two linear layers of the MLP in each transformer module. The parameters a and b are frozen while A and B are trainable.

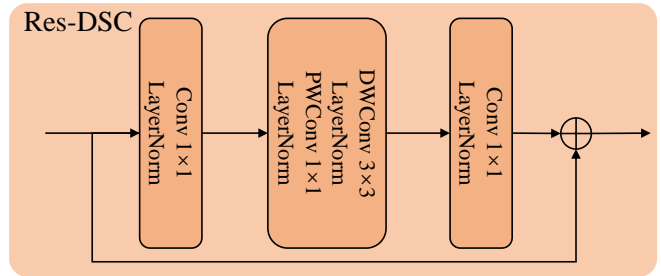


Fig. 4. The detailed structure of the Res-DSC module.

they can still learn effectively even when their parameters are projected into smaller, random subspaces. Inspired by this, LoRA was proposed, assuming that weight updates during adaptation also have low "intrinsic rank" [14]. For a pre-trained weight matrix $W_0 \in \mathbb{R}^{m \times n}$, its update can be represented using low-rank decomposition as $W_0 + \Delta W = W_0 + BA$, and the modified forward pass is:

$$h = W_0 x + \Delta W x = W_0 x + BAx \quad (2)$$

where $B \in \mathbb{R}^{m \times r}$ and $A \in \mathbb{R}^{r \times n}$, with $\text{rank } r \ll \min(m, n)$. During training, W_0 is frozen and does not receive gradient updates, while A and B are trainable. In this way, the pre-trained model weights are frozen, and the trainable low-rank decomposition matrices are injected into each layer of the transformer architecture, significantly reducing the number of trainable parameters for downstream tasks.

Recent studies have demonstrated the remarkable effectiveness of using random weights in deep learning models. On the one hand, introducing random vectors can significantly enhance a model’s adaptive capability, providing an effective mechanism for adjusting the model’s behavior without the need for extensive retraining or parameter tuning [15], [16]. On the other hand, several advanced deep learning techniques, including those focused on feature learning and transformations, rely heavily on affine transformations of learned features. Freezing these randomly initialized parameters has been shown to improve the network’s ability to

capture and generalize these affine transformations more effectively [25]. Additionally, in monocular depth estimation tasks, an inherent challenge is scale ambiguity, as depth information can vary in different contexts. Introducing random vectors specifically for scale adjustment can greatly improve the model’s flexibility, enabling it to better adapt to varying scales during inference. Inspired by these insights, we propose a novel and parameter-efficient fine-tuning method: low-rank adaptation based on random vectors (RVLoRA).

Fig. 3 illustrates the detailed structure of RVLoRA. This method builds on LoRA by adding randomly initialized vectors a and b , scaling the low-rank matrix to enhance the model’s adaptability to different scales. During training, we employ Kaiming uniform initialization [26] for a , b , and A while the low-rank matrices B are initialized to zeros to ensure that the weight matrix remains unaffected during the first forward pass. The frozen scaling vectors and the trainable low-rank matrices are combined with the original weights without incurring additional inference delay. Our method can be represented as:

$$h = W_0x + \Delta Wx = W_0x + \Lambda_b B \Lambda_a A x \quad (3)$$

where $B \in \mathbb{R}^{m \times r}$, $A \in \mathbb{R}^{r \times n}$, $\Lambda_b \in \mathbb{R}^{m \times m}$, $\Lambda_a \in \mathbb{R}^{r \times r}$, with rank $r \ll \min(m, n)$. In this method, the low-rank matrices B and A are trainable, while the scaling vectors $b \in \mathbb{R}^{m \times 1}$ and $a \in \mathbb{R}^{r \times 1}$ are randomly initialized and remain frozen during training. These vectors are formally represented as diagonal matrices Λ_b and Λ_a . This approach effectively performs random scaling on the rows of the low-rank matrices B and A , thereby enhancing the model’s adaptability across layers.

2) *Residual Block Based on Depthwise Separable Convolution (Res-DSC)*: Transformers offer advantages like dynamic attention, global context awareness, and strong generalization capabilities. However, they often struggle to extract fine details and local features. On the other hand, convolutions excel at capturing local features and come with inherent benefits such as shift, scale, and distortion invariance, though they are limited in their ability to perceive global context. Therefore, integrating CNNs with Transformers can create a synergistic effect, significantly enhancing the overall model performance.

Inspired by this, we designed a residual block based on depthwise separable convolution (Res-DSC), as illustrated in Fig. 4. This structure consists of three convolutional layers: the first layer is a 1×1 convolution to reduce the number of channels; the second layer is a 3×3 depthwise separable convolution which has fewer parameters, leading to not only faster computation but also a more streamlined model compared to traditional convolution; the final layer is a 1×1 convolution to restore the number of channels. To reduce the model’s parameters while ensuring the accuracy of depth estimation, we only add Res-DSC after the 3rd, 6th, 9th, and 12th transformer blocks. In Fig. 2, only the Res-DSC blocks after the 9th and 12th transformer blocks are shown, while the others are omitted for brevity.

TABLE I

THE CALCULATION OF APPLIED EVALUATION METRICS, IN WHICH d REPRESENTS THE PREDICTION DEPTH AND d^* REPRESENTS THE GROUND TRUTH.

Metric	Definition
Abs Rel	$\frac{1}{ N } \sum_{d \in N} d - d^* / d^*$
Sq Rel	$\frac{1}{ N } \sum_{d \in N} d - d^* ^2 / d^*$
RMSE	$\sqrt{\frac{1}{ N } \sum_{d \in N} (d - d^*)^2}$
RMSE log	$\sqrt{\frac{1}{ N } \sum_{d \in N} (\ln d - \ln d^*)^2}$
δ	$\frac{1}{ N } \left\{ d \in N \mid \max\left(\frac{d}{d^*}, \frac{d^*}{d}\right) < 1.25 \right\} \times 100\%$

3) *Decoder*: The decoder part adopts the same structure as Depth Anything Model [12]. The features from the last four layers of the encoder are fed into the decoder. Through the frozen Reassemble & Fusion module in the decoder, features at different resolutions are obtained and then aggregated. These aggregated features are then fed into the trainable Depth-Head module for the final dense prediction, resulting in depth estimation outputs at four scales.

C. Total Training Framework

We integrated our depth estimation network within the IID-SfMLearner framework [6]. In this framework, the intrinsic decomposition module performs intrinsic decomposition of the images, using decomposing-synthesis loss L_{ds} and albedo loss L_a to ensure the accuracy of the decomposition results and reflectance consistency between adjacent frames. The synthesis reconstruction module flexibly adjusts the illumination map and utilizes the decomposition results of the source image to reconstruct the target image, introducing mapping-synthesis loss L_{ms} to supervise network training.

Besides, we apply an edge-aware depth smooth loss L_{es} [27] to enhance smoothness in non-edge regions while preserving sharp edges and details:

$$L_{es}(D_t, I_t) = |\partial_x D_t| e^{-|\partial_x I_t|} + |\partial_y D_t| e^{-|\partial_y I_t|} \quad (4)$$

where ∂D_t and ∂I_t are the first derivative of the depth map D_t and the target image I_t . The final loss function is defined as:

$$loss = \lambda_{ds} L_{ds} + \lambda_a L_a + \lambda_{ms} L_{ms} + \lambda_{es} L_{es} \quad (5)$$

where λ_{ds} , λ_a , λ_{ms} and λ_{es} are weighting factors.

IV. EXPERIMENT

A. Implementation Details

All models are implemented using PyTorch [28] and trained end-to-end using the Adam optimizer [29] with $\beta_1 = 0.9$ and $\beta_2 = 0.999$. We train for 30 epochs on a GeForce RTX 3090 GPU with a batch size of 8. The initial learning rate is set to 1×10^{-4} and is multiplied by a scale factor of 0.1 after 10 epochs. In our experiments, the rank for RVLoRA is set to 4, the loss weights λ_{ds} , λ_a , λ_{ms} , and λ_{es} are set to 0.2, 0.2, 1, and 0.01, respectively.

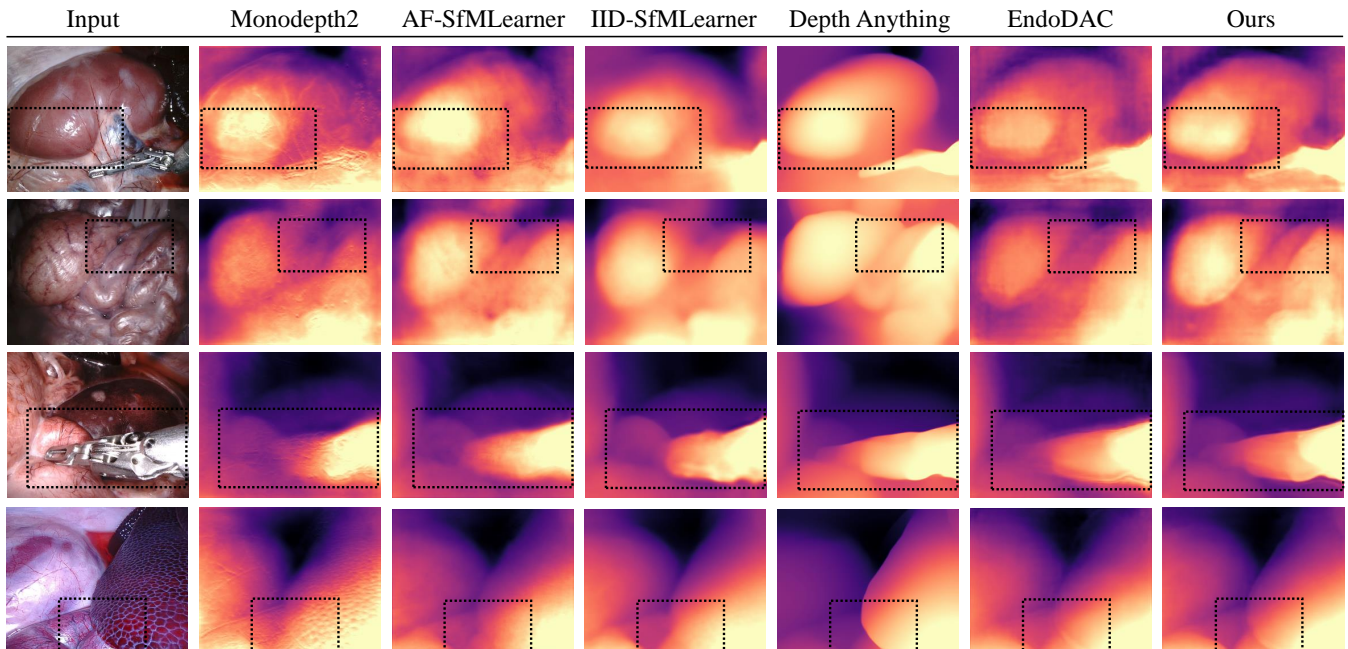


Fig. 5. The visual results of the comparative experiments. It is evident that our method performs better in capturing details such as object edges. In particular, the regions highlighted by the black boxes demonstrate a significant advantage of our approach. Note: Since the ground truth in this dataset is captured using structured light encoding, comparing it with the depth map visually is not intuitive. As with other papers [7], [6], [13], we do not present the ground truth for comparison.

TABLE II
COMPARATIVE EXPERIMENTAL RESULTS ON THE SCARED DATASET. THE BEST RESULTS ARE PRESENTED IN BOLD.

Method	Source	Abs Rel↓	Sq Rel↓	RMSE↓	RMSE log↓	$\delta \uparrow$	Total.(M)	Train.(M)
SfMLearner [4]	CVPR'17	0.086±0.037	1.021±1.100	7.553±5.110	0.121±0.060	0.925±0.081	31.60	31.60
Monodepth2 [5]	ICCV'19	0.066±0.025	0.577±0.482	5.781±3.174	0.093±0.036	0.961±0.043	14.84	14.84
Endo-SfMLearner [20]	MedIA'21	0.068±0.029	0.679±0.709	6.227±4.137	0.098±0.047	0.955±0.054	14.84	14.84
AF-SfMLearner [7]	MedIA'22	0.060±0.024	0.443±0.347	4.964±2.348	0.082±0.032	0.973±0.037	14.84	14.84
IID-SfMLearner [6]	JBHI'24	0.058±0.026	0.435±0.375	4.820±2.583	0.080±0.035	0.969±0.043	14.84	14.84
Depth Anything [12]	CVPR'24	0.086±0.039	0.927±0.875	6.957±3.817	0.112±0.049	0.929±0.089	97.50	97.50
EndoDAC [13]	MICCAI'24	0.051±0.022	0.355±0.334	4.442±2.509	0.073±0.032	0.979±0.032	99.09	1.66
Ours	-	0.048±0.021	0.315±0.297	4.172±2.261	0.068±0.030	0.982±0.027	98.80	1.38

B. Dataset and Metrics

We conducted our experiments on the SCARED dataset, which was collected using the da Vinci Xi endoscope during the dissection of fresh pig abdomens [30]. High-quality depth ground truth was obtained using structured light encoding during the acquisition process. Following the splitting strategy in prior works [6], [7], we divided the SCARED dataset into 15,351 frames for training, 1,705 frames for validation, and 551 frames for testing.

We adopted commonly used evaluation metrics such as Abs Rel, Sq Rel, RMSE, RMSE log, and Threshold δ , with their calculation formulas shown in Table I. Similar to previous methods [6], [7], during the evaluation, we scale the predicted depth map via the median scaling, which can be expressed as:

$$D_{scaled} = d * (median(d^*) / median(d)) \quad (6)$$

where d and d^* represents the predicted depth and the ground truth, respectively. The upper limit for scaling the depth map is set to 150 millimeters, which effectively covers

almost all pixels in the SCARED dataset.

C. Comparison Experiments

We compared our method with seven competitive unsupervised depth estimation methods: SfMLearner [4], Monodepth2 [5], Endo-SfMLearner [20], AF-SfMLearner [7], IID-SfMLearner [6], Depth Anything [12], and EndoDAC [13]. Among these, EndoDAC is currently the state-of-the-art method on the SCARED dataset. The first three methods are reproduced from scratch following the code provided by the authors, and the last four methods are tested using the optimal model provided by the authors. Table II presents the results of the comparative experiments.

SfMLearner and Monodepth2, which are designed for natural scenes, perform poorly on endoscopic images. While Endo-SfMLearner, AF-SfMLearner, and IID-SfMLearner have introduced algorithmic improvements tailored to the unique characteristics of endoscopic images, their performance gains remain limited. Depth Anything Model, the latest foundation model for depth estimation, also falls short due to the absence of medical images in its training datasets.

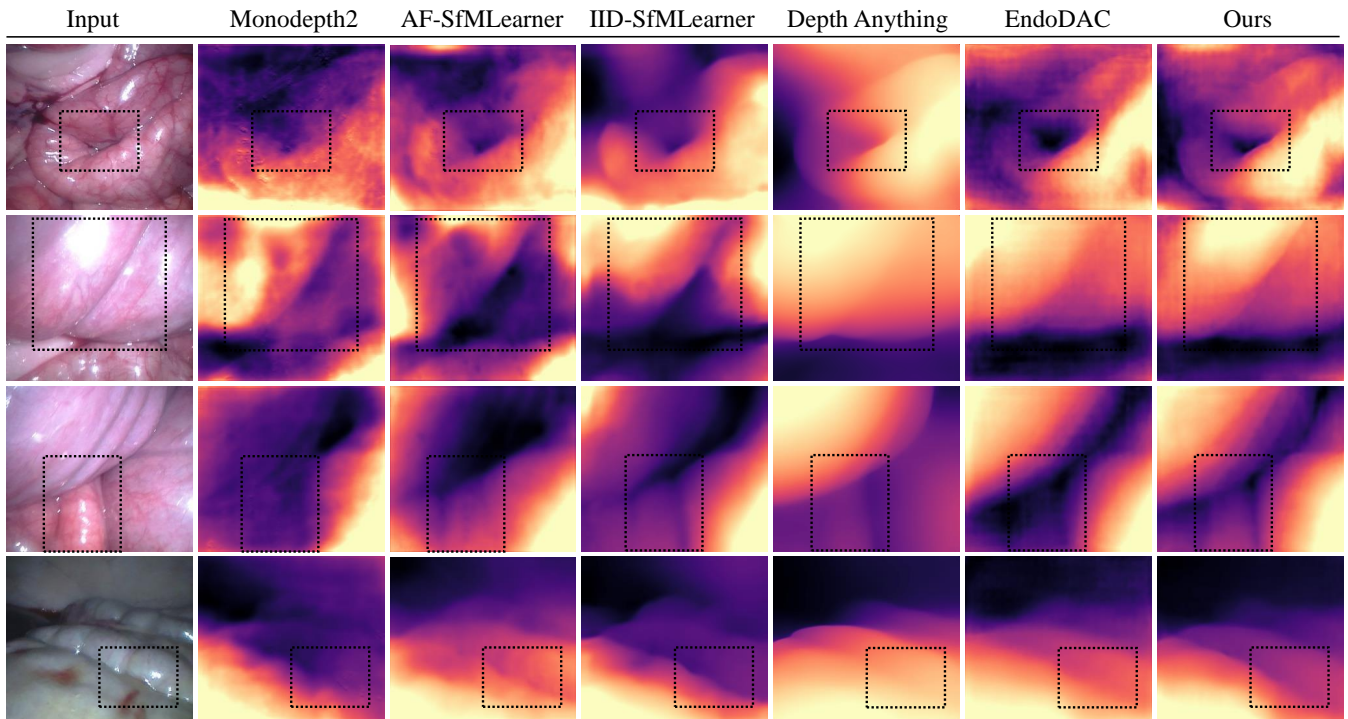


Fig. 6. Qualitative comparison of applying the model trained on the SCARED dataset to the Hamlyn dataset for validation without any fine-tuning. Our method not only avoids erroneous estimates but also delivers more precise details. The regions highlighted by the black boxes illustrate a notable advantage of our approach, further demonstrating its strong generalization ability.

TABLE III
THE COMPARISON OF FINE-TUNING STRATEGIES

Fine-tuning strategy	Abs Rel↓	Sq Rel↓	RMSE↓	RMSE log↓	$\delta \uparrow$
LoRA [14]	0.051	0.349	4.383	0.072	0.978
VeRA [15]	0.054	0.404	4.706	0.076	0.977
DVLoRA [13]	0.050	0.340	4.323	0.071	0.981
Ours	0.048	0.315	4.172	0.068	0.982

EndoDAC, which similarly fine-tunes the Depth Anything Model, has achieved significant improvements over earlier methods. In comparison, our method outperforms all others across various metrics. Notably, our approach has the fewest trainable parameters, totaling only 1.38M, which accounts for just 1.4% of the overall parameters.

Fig. 5 presents some representative results for the compared methods. It can be observed that the depth maps estimated by our method are smoother and more continuous, with better performance at object boundaries, indicating that our method exhibits superior performance in capturing image detail information.

Additionally, we compared our method with other fine-tuning strategies, and the results are presented in Table III. It is evident that our approach provides the optimal fine-tuning for the depth estimation foundation model.

Like other methods [7], to further test the generalization ability of the proposed method, we directly applied the model trained on SCARED to the Hamlyn dataset for validation without any fine-tuning. The Hamlyn dataset is a laparoscopic/endoscopic video dataset created by the Hamlyn Centre at Imperial College London, containing rich laparoscopic

TABLE IV
EXPERIMENTAL RESULTS ON THE HAMLYN DATASET. THE BEST RESULTS ARE PRESENTED IN BOLD.

Method	Abs Rel↓	Sq Rel↓	RMSE↓	RMSE log↓	$\delta \uparrow$
AF-SfMLearner [7]	0.130	2.134	11.306	0.165	0.843
IID-SfMLearner [6]	0.120	1.833	10.362	0.156	0.867
EndoDAC [13]	0.103	1.422	9.082	0.130	0.906
Ours	0.094	1.215	8.318	0.120	0.924

and endoscopic video data [31].

The test results on Hamlyn dataset are shown in the Table IV. We only compare with a few of the most competitive methods. It can be seen that our method demonstrates strong generalization ability and continues to achieve state-of-the-art performance on this dataset. The visual results, as shown in the Fig. 6, clearly illustrate that the depth maps generated by our method exhibit greater continuity and superior performance in capturing object boundaries and texture details. This experiment provides strong evidence of the robust generalization capability of our approach.

D. Ablation Study

To further demonstrate the effectiveness of the proposed modules, ablation experiments were conducted and the results are shown in Table V. The first row in the table represents the results obtained by directly testing the Depth Anything Model without any fine-tuning. The subsequent rows show the results of progressively adding the proposed two modules. The experimental results indicate that both modules effectively improve the depth estimation perfor-

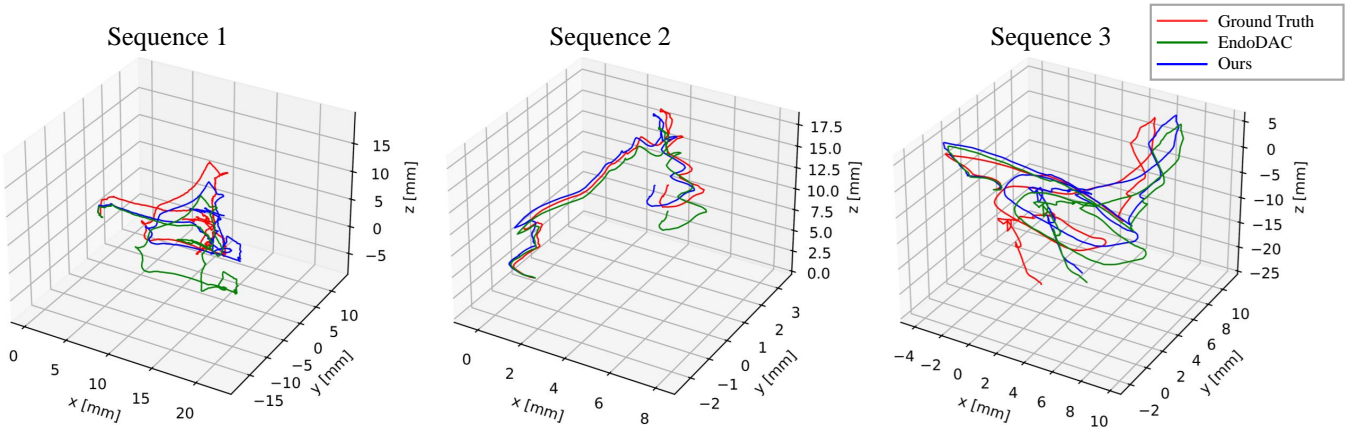


Fig. 7. Visualization of pose estimation results. The red line represents the ground truth, the green line represents the result from EndoDAC, and the blue line represents our method’s result. It can be observed that our results exhibit less trajectory drift and align more closely with the ground truth.

TABLE V
THE ABLATION STUDY RESULTS.

RVLoRA	Res-DSC	Abs Rel↓	Sq Rel↓	RMSE↓	RMSE log↓	δ ↑
×	×	0.086	0.927	6.957	0.112	0.929
✓	×	0.052	0.351	4.382	0.074	0.977
×	✓	0.056	0.415	4.788	0.078	0.974
✓	✓	0.048	0.315	4.172	0.068	0.982

TABLE VI
THE ABLATION STUDY ON THE NUMBER OF RES-DSC MODULES

Num of Res-DSC	Abs Rel↓	Sq Rel↓	RMSE↓	RMSE log↓	δ ↑
2	0.052	0.358	4.420	0.073	0.975
3	0.052	0.345	4.360	0.073	0.976
4	0.048	0.315	4.172	0.068	0.982
6	0.050	0.344	4.284	0.070	0.982

TABLE VII
THE RESULTS OF POSE ESTIMATION.

Method	ATE (Seq 1)↓	ATE (Seq 2)↓	ATE (Seq 3)↓
EndoDAC [13]	0.0521	0.0390	0.0779
Ours	0.0505	0.0371	0.0771

mance.

In our method, the Res-DSC modules are evenly distributed across the 12 transformer modules of the encoder. For instance, when using three Res-DSC modules, they are placed at the 4th, 8th, and 12th layers. To determine the optimal number of Res-DSC modules, we conducted a series of ablation experiments. The results, shown in Table VI, indicate that using four Res-DSC modules achieves the best performance while maintaining a relatively low parameter count.

E. Pose Estimation

In unsupervised monocular depth estimation, camera pose estimation and depth estimation are jointly learned tasks, where the accuracy of the pose network’s estimations can also indirectly reflect the precision of the depth estimation. Therefore, we also evaluated the performance of the pose network on the SCARED dataset. We assessed three video sequences using the Absolute Trajectory Error (ATE) met-

ric, comparing our results only with the most competitive method, EndoDAC [13]. The quantitative results are presented in Table VII, where our method outperforms the compared method across the three sequences. The visual results, shown in Fig. 7, demonstrate reduced trajectory drift and a closer alignment with the ground truth for our method. This further validates the effectiveness of our depth estimation approach.

V. CONCLUSIONS

In this work, we apply foundation models to the task of endoscopic image depth estimation. To address the challenge of limited medical image data and the inability to train foundation models from scratch, we propose a low-rank adaptation module based on random vectors to fine-tune existing depth estimation foundation model. We introduce a residual block based on depthwise separable convolution to enhance the network’s capability to capture local features. Comparative experiments show that our method achieves state-of-the-art performance on the SCARED dataset with the minimum number of trainable parameters. The experimental results on the Hamlyn dataset further validate the strong generalization ability of our method. Ablation studies validate the effectiveness of the proposed modules, and the favorable results from the pose estimation experiments further reflect the accuracy of our approach. Integrating this method into augmented reality navigation systems for minimally invasive endoscopic surgery could enhance surgeons’ spatial awareness of the internal anatomy, thereby improving the safety and precision of the surgical procedure.

Meanwhile, our method has certain limitations in inference time. The large number of parameters in the foundational model results in longer inference times compared to conventional methods. Through testing, our method achieves an average inference time of 30ms per image, with a frame rate of 33 frames per second, which is sufficient to meet real-time requirements. Future work could explore further optimization of the network architecture to achieve more efficient depth estimation.

REFERENCES

- [1] S. Leonard, A. Sinha, A. Reiter, M. Ishii, G. L. Gallia, R. H. Taylor, and G. D. Hager, "Evaluation and stability analysis of video-based navigation system for functional endoscopic sinus surgery on in vivo clinical data," *IEEE Transactions on Medical Imaging*, vol. 37, no. 10, pp. 2185–2195, Oct. 2018.
- [2] Y. Chu, X. Li, X. Yang, D. Ai, Y. Huang, H. Song, Y. Jiang, Y. Wang, X. Chen, and J. Yang, "Perception enhancement using importance-driven hybrid rendering for augmented reality based endoscopic surgical navigation," *Biomedical Optics Express*, vol. 9, no. 11, pp. 5205–5226, 2018.
- [3] Z. Liu, C. Song, J. Cheng, J. Luo, and X. Wang, "Self-supervised monocular depth estimation with effective feature fusion and self distillation," in *2024 IEEE/RSJ International Conference on Intelligent Robots and Systems (IROS)*, 2024, pp. 7160–7166.
- [4] T. Zhou, M. Brown, N. Snaveley, and D. G. Lowe, "Unsupervised learning of depth and ego-motion from video," in *Proceedings of the IEEE/CVF Conference on Computer Vision and Pattern Recognition*, pp. 1851–1858, 2017.
- [5] C. Godard, O. Mac Aodha, M. Firman, and G. J. Brostow, "Digging into self-supervised monocular depth estimation," in *Proceedings of the IEEE/CVF International Conference on Computer Vision*, pp. 3828–3838, 2019.
- [6] B. Li, B. Liu, M. Zhu, X. Luo, and F. Zhou, "Image intrinsic-based unsupervised monocular depth estimation in endoscopy," *IEEE Journal of Biomedical and Health Informatics*, 2024.
- [7] S. Shao, Z. Pei, W. Chen, W. Zhu, X. Wu, D. Sun, and B. Zhang, "Self-supervised monocular depth and ego-motion estimation in endoscopy: Appearance flow to the rescue," *Medical Image Analysis*, vol. 77, p. 102338, 2022.
- [8] A. Kolides, A. Nawaz, A. Rathor, D. Beeman, M. Hashmi, S. Fatima, D. Berdik, M. Al-Ayyoub, and Y. Jararweh, "Artificial intelligence foundation and pre-trained models: Fundamentals, applications, opportunities, and social impacts," *Simulation Modelling Practice and Theory*, vol. 126, p. 102754, 2023.
- [9] A. Kirillov, E. Mintun, N. Ravi, H. Mao, C. Rolland, L. Gustafson, T. Xiao, S. Whitehead, A. C. Berg, W.-Y. Lo, *et al.*, "Segment anything," in *Proceedings of the IEEE/CVF International Conference on Computer Vision*, pp. 4015–4026, 2023.
- [10] A. Agarwal and C. Arora, "Depthformer: Multiscale vision transformer for monocular depth estimation with global local information fusion," in *2022 IEEE International Conference on Image Processing (ICIP)*, pp. 3873–3877, IEEE, 2022.
- [11] A. Radford, J. W. Kim, C. Hallacy, A. Ramesh, G. Goh, S. Agarwal, G. Sastry, A. Askell, P. Mishkin, J. Clark, *et al.*, "Learning transferable visual models from natural language supervision," in *International conference on machine learning*, pp. 8748–8763, PMLR, 2021.
- [12] L. Yang, B. Kang, Z. Huang, X. Xu, J. Feng, and H. Zhao, "Depth anything: Unleashing the power of large-scale unlabeled data," in *Proceedings of the IEEE/CVF Conference on Computer Vision and Pattern Recognition*, pp. 10371–10381, 2024.
- [13] B. Cui, M. Islam, L. Bai, A. Wang, and H. Ren, "Endodac: Efficient adapting foundation model for self-supervised depth estimation from any endoscopic camera," *arXiv preprint arXiv:2405.08672*, 2024.
- [14] E. J. Hu, Y. Shen, P. Wallis, Z. Allen-Zhu, Y. Li, S. Wang, L. Wang, and W. Chen, "Lora: Low-rank adaptation of large language models," *arXiv preprint arXiv:2106.09685*, 2021.
- [15] D. J. Kopiczko, T. Blankevoort, and Y. M. Asano, "Vera: Vector-based random matrix adaptation," in *12th International Conference on Learning Representations*.
- [16] K. Lu, A. Grover, P. Abbeel, and I. Mordatch, "Frozen pretrained transformers as universal computation engines," in *Proceedings of the AAAI conference on artificial intelligence*, vol. 36, pp. 7628–7636, 2022.
- [17] H. Wu, B. Xiao, N. Codella, M. Liu, X. Dai, L. Yuan, and L. Zhang, "Cvt: Introducing convolutions to vision transformers," in *Proceedings of the IEEE/CVF international conference on computer vision*, pp. 22–31, 2021.
- [18] C. Si, W. Yu, P. Zhou, Y. Zhou, X. Wang, and S. Yan, "Inception transformer," *Advances in Neural Information Processing Systems*, vol. 35, pp. 23495–23509, 2022.
- [19] Y. Zheng, C. Zhong, P. Li, H.-a. Gao, Y. Zheng, B. Jin, L. Wang, H. Zhao, G. Zhou, Q. Zhang, and D. Zhao, "Steps: Joint self-supervised nighttime image enhancement and depth estimation," in *2023 IEEE International Conference on Robotics and Automation (ICRA)*, pp. 4916–4923, 2023.
- [20] K. B. Ozyoruk, G. I. Gokceler, T. L. Bobrow, G. Coskun, K. Incecan, Y. Almalioglu, F. Mahmood, E. Curto, L. Perdigoto, M. Oliveira, *et al.*, "Endoslam dataset and an unsupervised monocular visual odometry and depth estimation approach for endoscopic videos," *Medical Image Analysis*, vol. 71, p. 102058, 2021.
- [21] V. M. Batlle, J. Montiel, and J. D. Tardós, "Photometric single-view dense 3d reconstruction in endoscopy," in *2022 IEEE/RSJ International Conference on Intelligent Robots and Systems (IROS)*, 2022, pp. 4904–4910.
- [22] S. Hayou, N. Ghosh, and B. Yu, "LoRA+: Efficient low rank adaptation of large models," in *Forty-first International Conference on Machine Learning*, 2024.
- [23] Q. Zhang, M. Chen, A. Bukharin, P. He, Y. Cheng, W. Chen, and T. Zhao, "Adaptive budget allocation for parameter-efficient fine-tuning," in *The Eleventh International Conference on Learning Representations*, 2023.
- [24] A. Aghajanyan, S. Gupta, and L. Zettlemoyer, "Intrinsic dimensionality explains the effectiveness of language model fine-tuning," in *Proceedings of the 59th Annual Meeting of the Association for Computational Linguistics and the 11th International Joint Conference on Natural Language Processing*, pp. 7319–7328, Aug. 2021.
- [25] J. Frankle, D. J. Schwab, and A. S. Morcos, "Training batchnorm and only batchnorm: On the expressive power of random features in cnns," in *9th International Conference on Learning Representations*, May 2021.
- [26] K. He, X. Zhang, S. Ren, and J. Sun, "Delving deep into rectifiers: Surpassing human-level performance on imagenet classification," in *Proceedings of the IEEE international conference on computer vision*, pp. 1026–1034, 2015.
- [27] C. Godard, O. Mac Aodha, and G. J. Brostow, "Unsupervised monocular depth estimation with left-right consistency," in *Proceedings of the IEEE/CVF Conference on Computer Vision and Pattern Recognition*, pp. 270–279, 2017.
- [28] A. Paszke, S. Gross, F. Massa, A. Lerer, J. Bradbury, G. Chanan, T. Killeen, Z. Lin, N. Gimelshein, L. Antiga, A. Desmaison, A. Köpf, E. Yang, Z. DeVito, M. Raison, A. Tejani, S. Chilamkurthy, B. Steiner, L. Fang, J. Bai, and S. Chintala, "Pytorch: an imperative style, high-performance deep learning library," in *Proceedings of the 33rd International Conference on Neural Information Processing Systems*, (Red Hook, NY, USA), Curran Associates Inc., 2019.
- [29] D. P. Kingma and J. Ba, "Adam: A method for stochastic optimization," in *3rd International Conference on Learning Representations, ICLR 2015, San Diego, CA, USA, May 7-9, 2015, Conference Track Proceedings*, 2015.
- [30] M. Allan, J. Mcleod, C. Wang, J. C. Rosenthal, Z. Hu, N. Gard, P. Eisert, K. X. Fu, T. Zeffiro, W. Xia, *et al.*, "Stereo correspondence and reconstruction of endoscopic data challenge," *arXiv preprint arXiv:2101.01133*, 2021.
- [31] D. Recasens, J. Lamarca, J. M. Fácil, J. M. M. Montiel, and J. Civera, "Endo-depth-and-motion: Reconstruction and tracking in endoscopic videos using depth networks and photometric constraints," *IEEE Robotics and Automation Letters*, vol. 6, no. 4, pp. 7225–7232, 2021.